Cryogenics 116 (2021) 103282

Contents lists available at ScienceDirect

Cryogenics

journal homepage: www.elsevier.com/locate/cryogenics

Research paper

Investigations on a 1 K hybrid cryocooler composed of a four-stage Stirling-type pulse tube cryocooler and a Joule-Thomson cooler. Part A: Theoretical analyses and modeling

Tao Zhang [a,c], Haizheng Dang [a,b,c,d,*]

[a] State Key Laboratory of Infrared Physics, Shanghai Institute of Technical Physics, Chinese Academy of Sciences, 500 Yutian Road, Shanghai 200083, China
[b] Shanghai Research Center for Quantum Sciences, Shanghai 201315, China
[c] University of Chinese Academy of Sciences, Beijing 100049, China
[d] Shanghai Boreas Cryogenics Co., Ltd, Shanghai 201802, China

ARTICLE INFO

Keywords:
1 K hybrid cryocooler
Four-stage Stirling-type pulse tube cryocooler
Joule-Thomson cooler
Working mechanism
Theoretical analyses and modeling

ABSTRACT

This paper conducts systematic theoretical analyses of a hybrid cryocooler composed of a four-stage Stirling-type pulse tube cryocooler (SPTC) and a Joule-Thomson cooler (JTC), in which the former provides the necessary precooling powers to the latter which aims at reaching a temperature of 1.0 K. The structural design of the hybrid cryocooler is described and its working mechanism focused on. Both enthalpy flow and mass flow rate models are developed and then combined to study the cooling performance. The ideal gross cooling capacity and its changing characteristics with both the last stage precooling temperature and the upstream pressure are elaborated. It is found that the optimal last stage precooling temperature provided by the four-stage SPTC should be around 8.0 K with the optimal upstream pressure of 0.36 MPa to maximize the gross cooling capacity of the hybrid cryocooler at the aimed temperature. Finally, the heat exchanger efficiency of the JTC is considered to study the hybrid cryocooler performance close to the real situation. Given the last stage heat exchanger efficiency of 97%, with He-4 in the four-stage SPTC and He-3 in the JTC, a cooling power of 14.7 mW at 1.0 K can be achieved. The results indicate that the suggested hybrid cryocooler would become a promising candidate for cooling the superconducting nanowire single photon detector (SNSPD) for the potential applications in the next-generation space quantum information technology.

1. Introduction

The past decade has witnessed the rapid development of the space quantum information technology [1,2], in which the single photon detector (SPD) plays an important role in quantum key distribution and space quantum communication, etc. At present, most practical SPDs are made from semiconducting materials, of which the Si single-photon avalanche diode (SPAD) and the InGaAs/InP SPAD [3] are widely used and they do not require the cryogenic working environment. The SPDs can also be fabricated by superconducting materials, such as the transition edge sensor (TES) [4], superconducting tunnel junction (STJ) [5], microwave kinetic inductance detector (MKID) [6] and superconducting nanowire single-photon detector (SNSPD) [7,8], of which the SNSPD exhibits the striking characteristics of high detection efficiency, low dark count rate, high speed and low timing jitter, and thus be suggested as a promising new generation SPD for the quantum information technology.

Unlike the TES, the SNSPD does not require the demanding sub-Kelvin operating temperature. However, it does need a considerably low temperature of 1–2 K to work properly. The normal operating temperature of a typical SNSPD is usually around 2 K with the required cooling power of milliwatt-class. In practice, a lower temperature close to 1 K is often required to further improve its performance for the following two reasons. First, the decrease of temperature from 2.2 K to near 1 K can result in the dark count rate of the SNSPD reducing by magnitude, such as from $10^3\ s^{-1}$ to $10^2\ s^{-1}$ [9]. Second, there are always some irreversible losses when the SNSPD is coupled with the cryocooler, and thus a cryocooler capable of lower temperatures than 2 K will make sure that the SNSPD works at the desirable temperature.

The cooling temperature of 1–2 K still poses a serious challenge to the associated cryogenic system. The superfluid liquid helium Dewar,

* Corresponding author at: State Key Laboratory of Infrared Physics, Shanghai Institute of Technical Physics, Chinese Academy of Sciences, 500 Yutian Road, Shanghai 200083, China.
E-mail address: haizheng.dang@mail.sitp.ac.cn (H. Dang).

https://doi.org/10.1016/j.cryogenics.2021.103282
Received 27 July 2020; Received in revised form 9 February 2021; Accepted 24 February 2021
Available online 9 March 2021

Nomenclature

A	area (m^2)
C_p	isobaric specific heat (kJ kg^{-1} K^{-1})
CHEX	counterflow heat exchanger
d	orifice diameter (μm)
G	mass flux (kg m^{-2} s^{-1})
h	specific enthalpy (kJ kg^{-1})
Δh_T	integral isothermal Joule-Thomson effect (kJ kg^{-1})
IT	inertance tube
$\dot{m}$	mass flow rate (mg s^{-1})
M	molecular mass (kg mol^{-1})
P	pressure (Pa)
PHEX	precooling heat exchanger
PT	pulse tube
q_C	specific cooling capacity (kJ kg^{-1})
q_L	latent heat (kJ kg^{-1})
Q_C	gross cooling capacity (mW)
Q_{pre}	precooling capacity (mW)
R	universal gas constant(8.314 J mol^{-1} K^{-1})
Reg	regenerator
s	specific entropy (kJ kg^{-1} K^{-1})
T_C	cooling temperature (K)
T_H	ambient temperature (K)
T_{pre}	precooling temperature (K)
V	velocity (m s^{-1})

Greeks

Γ	ratio of real gas choked mass flux to that of ideal gas
η	efficiency of CHEX
κ	ideal gas ratio of isobaric to isochoric heat capacities
ρ	density (kg/m^3)

Subscripts

0	stagnation conditions
1,2,3…	thermodynamic states in Fig. 1 and Fig. 2
D	downstream, low pressure of JT cycle
opt	optimum
U	upstream, high pressure of JT cycle

Superscripts

ID	ideal gas

together with the additional decompression technology, can produce the aimed temperature. However, due to the evaporation losses, it has to be refilled frequently, which often results in the short continuous working time and also an expensive cryogenic system. Furthermore, for some special environment such as in space, a huge Dewar is unacceptable and the refilling usually impossible.

Some multi-stage cryocoolers have the potential for providing the aimed cryogenic environment continuously and more cheaply. For example, at present, several commercial two-stage Gifford-McMahon (GM) cryocoolers can achieve a minimum no-load temperature of about 2.1 K, which is often slightly higher than the optimum operating temperature of the SNSPD if the necessary cooling power is considered. The GM cryocoolers also exist several substantial disadvantages in terms of the high vibration level and the severe wear generated by the moving component at the cold head which often limits its continuous operation time to about 8000 h. Moreover, it is impossible to be used in orbit because of its enormous weight and huge input power.

In contrast to the GM cryocooler, the pulse tube cryocooler (PTC) has no any moving component at the cold end, from which it gains the obvious advantages in high reliability, long life and low vibration at the cold end [10,11]. The Stirling-type PTC (SPTC) [12] driven by the linear compressor further achieves the long continuous operation time at the warm end, and thus results in an attractive cryocooler candidate for space applications.

However, for the SPTC operating at high frequencies of over 20 Hz, the aimed cooling temperature of around 2 K is still a formidable challenge, even though the multi-stage arrangement is used. For example, Nast et al. [13] reported a four-stage SPTC reaching a no-load temperature of 3 K in 2008. A three-stage SPTC was reported to achieve 4.26 K in 2013 [14] and a multi-stage SPTC precooled by liquid nitrogen reaching 3.6 K reported in 2018 [15]. And then in 2020, Dang et al. [16,17] presented theoretical and experimental investigations of a four-stage SPTC achieving 3.3 K. Although in theory it is possible that a multi-stage SPTC can achieve cooling at a temperature of around 2 K provided with He-3 as the working fluid, both the regenerative feature of a SPTC and the substantial practical losses in a real system often make the goal unrealistic.

By contrast, the Joule-Thomson cooler (JTC), as a recuperative cryocooler, is much easier to acquire the required cooling at the temperatures of even below 2 K due to the characteristics of the isenthalpic expansion. Furthermore, similar to SPTC, there is also no any moving part at the cold end of the JTC, and the driver of the JTC is also similar to the linear compressor used by the SPTC, though the former uses the direct current compressor while the latter the alternating one instead. Therefore, if a JTC is added as the final stage to a multi-stage SPTC, it is expected that a hybrid cryocooler can be developed with higher cooling efficiencies at lower temperatures.

In practice, if a JTC was precooled by a two-stage GM cryocooler or a GM-type PTC, the expected low temperatures could be achieved relatively easier. For example, in 2014 Wang et al. [18] developed a closed-cycle cryostat composed of a GM-type PTC and a JTC reaching a no-load temperature of 1.62 K. And also several researchers reported their results with a JTC precooled by a two-stage GM cryocooler achieving the temperatures of 4.4 K [19] or 4.5 K [20], respectively. However, as already mentioned above, for some important applications, especially in orbit, the use of GM cryocooler or a GM-type PTC is infeasible. And thus the SPTC used for precooling becomes desirable.

Petach et al. [21,22] had coupled a JTC to a developed three-stage SPTC in 2009, by adding additional compression stages to the compressor and use of He-3 as the working fluid, the hybrid cryocooler could reach 1.7 K. In 2019, Dang et al. [23] also reported a similar hybrid cryocooler composed by a three-stage SPTC and a JTC which was expected to achieve 1.6 K for cooling the SNSPD. And now, due to the new breakthrough of the four-stage SPTC in the authors' laboratory which had reached 3.3 K in 2020 [16,17], a more ambitious plan is being formulated which is aimed to further lower the temperature to 1.0 K by coupling a multi-stage JTC to the developed four-stage SPTC.

This paper will present the design and performance based on the in-depth analyses of its working mechanism. A theoretical enthalpy flow model will be established to investigate the changing trend of the specific cooling capacity over the precooling temperature and the upstream pressure at the cooling temperature of 1.0 K. A gas mass flux map for He-3 over cooling temperature and upstream pressure will also be built to study the ideal gross cooling capacity. The working conditions of the JTC will be optimized. Finally, the heat exchanger efficiency of the JTC is considered to study the hybrid cryocooler performance close to the real situation. The working mechanism of the hybrid cryocooler will be clarified and systematic optimizations of its cooling performance summarized.

2. Hybrid cryocooler set-up

Fig. 1 shows a schematic of the set-up of the suggested hybrid cryocooler, which is composed of a four-stage SPTC and a JTC and the two parts are thermally coupled with each other.

The four-stage SPTC is driven by two moving-coil linear compressors, in which the first two stage pulse tube cold fingers (PTCFs) are driven by one compressor and the last two stage PTCFs by the other one [16,17]. Each stage of the PTCFs consists of regenerators, pulse tubes, inertance tubes, reservoirs and heat exchangers including warm and cold heads. The first three stage PTCFs all adopt the coaxial arrangement while the fourth stage uses in-line one. To achieve the very low temperature for the JTC, the last three cold heads are all serve as the precooling heat exchangers (PHEXs) and coupled with the JTC to provide precooling capacities Q_{pre1}, Q_{pre2}, Q_{pre3} at three different temperatures T_{pre1}, T_{pre2}, T_{pre3}, respectively.

The JTC consists of the four-stage JT compressors and the JT cold finger in which the latter is composed of the four-stage counter-flow heat exchangers (CHEXs), a JT valve, a bypass valve and an evaporator. The efficiencies of the four-stage CHEXs are η_1, η_2, η_3 and η_4, respectively. The four-stage JT compressors consist of four linear compressors which are cascaded together. These linear compressors are similar to those used in the four-stage SPTC, but the latter ones generate the oscillating sinusoidal flow while the former ones turn the oscillating flow into direct current (DC) flow by the reed valves used at the inlet and outlet.

As shown in Fig. 1, firstly, the four-stage SPTC starts to work and the temperatures of the three PHEXs gradually decrease. When the PHEX temperatures are stable, the JTC starts to operate with the bypass valve open while the JT valve closed. The pressure of working fluid is lifted by the JT compressors stage by stage, from P_D to P_U. The high pressure upstream flow with the mass flow rate $\dot{m}$ and temperature T_H enters the JT cold finger, exchanging heat with the low pressure downstream flow at the first three stage CHEXs and being precooled by the three stage PHEXs, then reaching the evaporator through the bypass valve. When the evaporator temperature is equal to T_{pre3}, the JT valve is opened while the bypass valve gets closed. The upstream flow enters the last stage CHEX and then passes through the JT valve. In this process, the pressure decreases from P_U to P_D, which is below the critical point, and produces a corresponding temperature drop δT due to the throttling effect. The enthalpy of the working fluid remains constant before and after expansion. In the evaporator, a part of the flow changes from gaseous to liquid. The latent heat of the liquid part is defined as the gross cooling capacity Q_C of the JTC. The lowest cooling temperature T_C corresponds to its saturated vapor pressure which is dependent on the downstream pressure P_D achieved by the JT compressor.

For the cooling temperature of 1.0 K by He-3, the corresponding saturated vapor pressure is about 1.16 kPa [24], which is much lower than the atmosphere pressure and thus also poses a real challenge to the design of the JT system. The pressure drops on the low pressure side of the actual JT system cannot be ignored. For example, in Ref. [25] and Ref. [26], the 1 K-class He-3 JT cooler had large pressure drops of 2.2 kPa and 4 kPa, respectively, occurred on the low pressure side under different working conditions, which prevented from acquiring a lower cooling temperature. However, there is much room to improve the situation and it is still feasible to reduce the pressure loss to a much smaller value and then meet the aimed 1.16 kPa provided that the appropriate effective approach is adopted. For instance, by enlarging the inner diameter of the low pressure side tube, namely the pump line, to 23.8

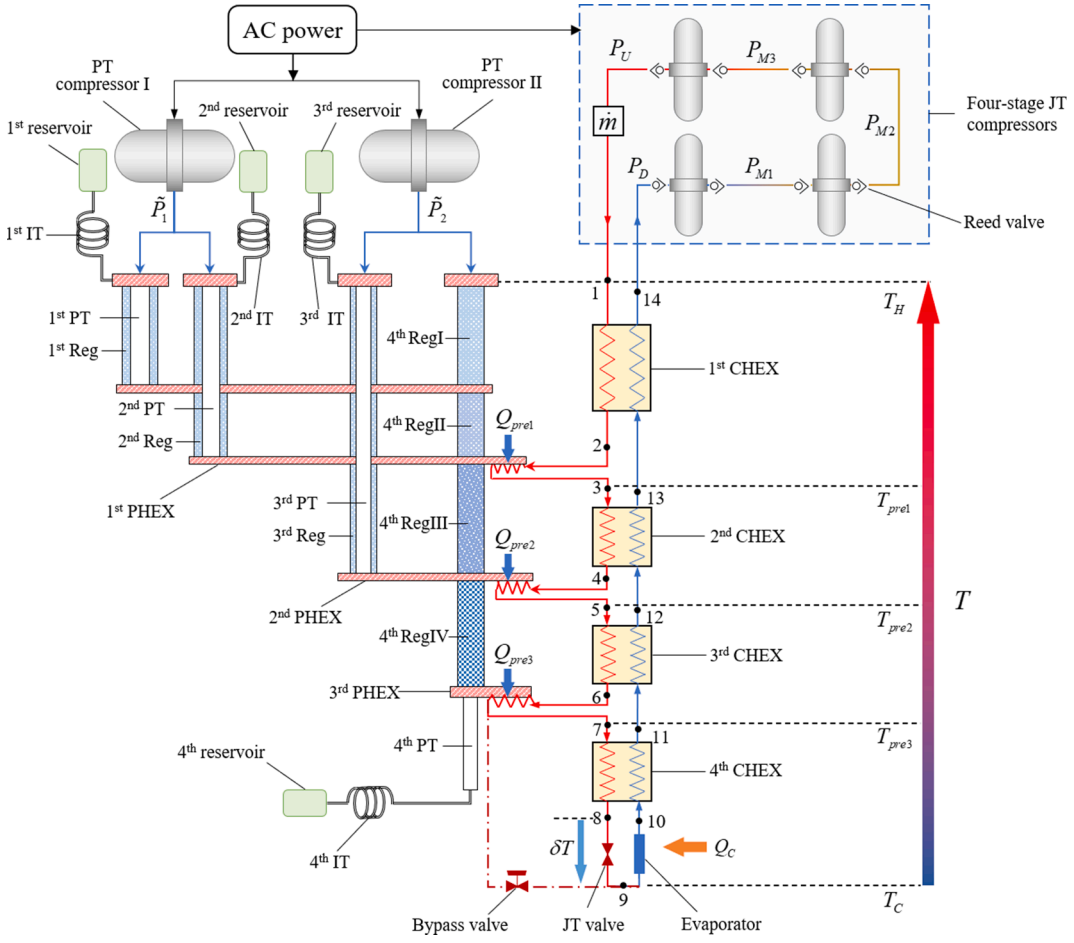

Fig. 1. Schematic of set-up of the developed hybrid cryocooler.

mm, Jahromi and Miller [27] had obtained a smaller pressure drop of less than 0.35 kPa and then achieved a lower temperature of 1.39 K with He-4, which meant the final low pressure after throttling reached around 0.4 kPa. This value was far lower than 1.16 kPa we required. In other words, if the used working fluid He-4 was replaced by He-3, with the same pressure drop of 0.35 kPa and a low pressure of 0.4 kPa, a final cooling temperature of 0.8 K could be expected. And furthermore, in practice, for He-3, one of the practical low-temperature limits that had already been obtained by reducing the vapor pressure was 0.3 K [28], which was much lower than 1 K. The corresponding saturation pressure of He-3 at 0.3 K was only about 0.2 Pa, which indicated that the pressure drop could be very small. Therefore, in reality, it is still feasible to achieve the required saturated vapor pressure on the low pressure side after throttling. Besides, it is also reasonable for ignoring the low pressure drop in the theoretical enthalpy flow model in the following section.

3. Enthalpy flow model

3.1. Thermodynamic cycle

Enthalpy is an important thermodynamic parameter in the hybrid cryocooler since it is closely related with both the gross cooling capacity of the JTC and the precooling performance of the SPTC. Fig. 2 shows the Linde-Hampson cycle of the JTC in the *P-h* thermodynamic plane, in which section 1–8 represents the recuperative cooling process while section 8–9 the isenthalpic expansion process by which the cooling temperature is achieved. Section 9–10 stands for the heat absorbing process where the cooling capacity is obtained while section 10–14 the recuperative heating process.

In Fig. 2, the point 1 represents the state at the inlet of the JTC and the upstream pressure channel of the first stage CHEX while point 2 is the state at the outlet from the first stage CHEX and the entrance to the first stage PHEX. Likewise, points 3, 5 and 7 are the states at the inlets of the second, third and fourth stage CHEXs, respectively, while points 4 and 6 are the states at the outlet from the second and third stage CHEXs, respectively. Points 8 and 9 represent the states before and after the throttling process which have the same enthalpy, respectively. Points 10–14 are the states of both ends of the four stages CHEXs along the downstream pressure channel, respectively. Besides, points 1D, 3D, 5D and 7D represent the states which have the same temperatures as those of points 1, 3, 5, 7 but are on the downstream pressure line, respectively.

The following assumptions are made to simplify the enthalpy flow analyses:

(1) Both P_U and P_D keep constants during the cycle, which indicates that the flow pressure drop is ignored on both upstream and downstream pressure sides;
(2) The cooling power is only provided at the evaporator and there is no any parasitic heat leak at all heat exchangers;
(3) The temperatures of the working fluid are equal to those of the PHEXs after precooling, which indicates that $T_3 = T_{pre1}$, $T_5 = T_{pre2}$ and $T_7 = T_{pre3}$.

The specific cooling capacity at the evaporator is defined as:

$$q_C = \frac{Q_C}{\dot{m}} = h_{10} - h_9 \tag{1}$$

where Q_C is the gross cooling capacity with the unit of mW and $\dot{m}$ is the mass flow rate with mg/s. According to the law of conservation of energy, the exchanged heat at the last stage CHEX, referred as the extent of recuperation, is given as follow:

$$\delta h_4 = h_{11} - h_{10} = h_7 - h_8 \tag{2}$$

Since $h_8 = h_9$, the specific cooling capacity can be written as:

$$q_C = \frac{Q_C}{\dot{m}} = h_{10} - h_9 = h_{10} - h_8 = h_{11} - h_7 \tag{3}$$

The efficiency of the fourth stage CHEX is defined as:

$$\eta_4 = \frac{h_{11} - h_{10}}{h_{7D} - h_{10}} \tag{4}$$

Hence, the specific cooling capacity can be expressed as:

$$q_C = h_{11} - h_7 = h_{10} - h_7 + \eta_4(h_{7D} - h_{10}) \tag{5}$$

Similarly, for the third stage CHEX, we get:

$$\delta h_3 = h_{12} - h_{11} = h_5 - h_6 \tag{6}$$

$$\eta_3 = \frac{h_{12} - h_{11}}{h_{5D} - h_{11}} \tag{7}$$

Based on the above two equations, h_6 is determined by:

$$h_6 = h_5 - \eta_3(h_{5D} - h_{11}) \tag{8}$$

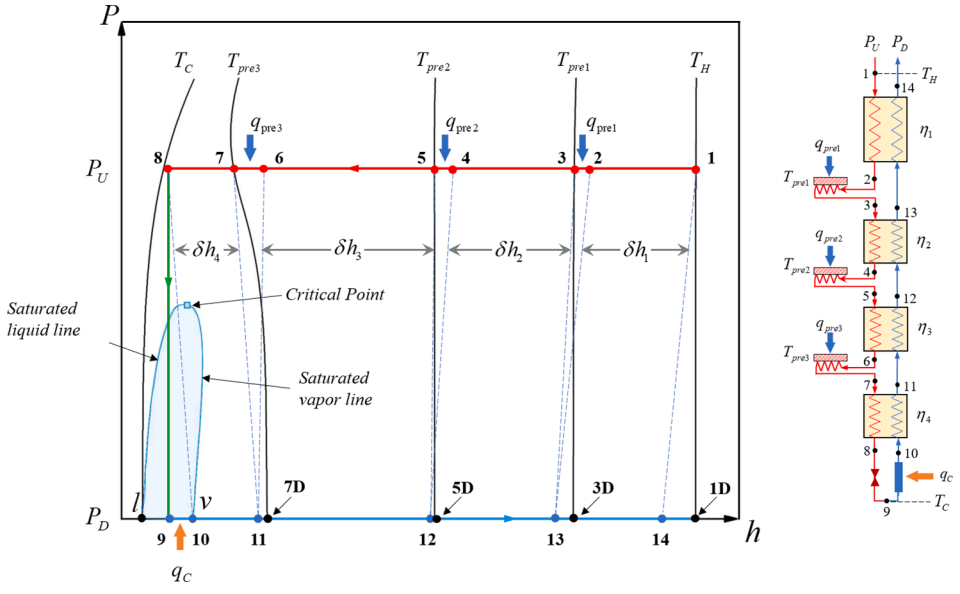

Fig. 2. Linde-Hampson cycle of JTC in *P-h* thermodynamic plane.

Therefore, the specific precooling capacity of the third stage PHEX is given as follow:

$$q_{pre3} = \frac{Q_{pre3}}{\dot{m}} = h_6 - h_7 = h_5 - h_7 - \eta_3(h_{5D} - h_{11}) \tag{9}$$

Substituting Eq. (4) into Eq. (9) and η_4 is introduced to eliminate the unknown h_{11}, then Eq. (9) becomes:

$$q_{pre3} = (h_5 - h_7) - \eta_3(h_{5D} - h_{10}) + \eta_3\eta_4(h_{7D} - h_{10}) \tag{10}$$

Similarly, the specific precooling capacities of the second and first stage PHEXs are derived as:

$$q_{pre2} = (h_3 - h_5) - \eta_2(h_{3D} - h_{10}) + \eta_2\eta_4(h_{7D} - h_{10}) + \eta_2\eta_3(h_{5D} - h_{10}) - \eta_2\eta_3\eta_4(h_{7D} - h_{10}) \tag{11}$$

$$q_{pre1} = (h_1 - h_3) - \eta_1(h_{1D} - h_{10}) + \eta_1\eta_4(h_{7D} - h_{10}) + \eta_1\eta_3(h_{5D} - h_{10}) - \eta_1\eta_3\eta_4(h_{7D} - h_{10}) + \eta_1\eta_2(h_{3D} - h_{10}) - \eta_1\eta_2\eta_4(h_{7D} - h_{10}) - \eta_1\eta_2\eta_3(h_{5D} - h_{10}) + \eta_1\eta_2\eta_3\eta_4(h_{7D} - h_{10}) \tag{12}$$

In order to find out the relationships between the cooling and precooling capacities, assuming the four stage CHEXs have the same efficiency:

$$\eta_1 = \eta_2 = \eta_3 = \eta_4 = \eta \tag{13}$$

Then the precooling capacities are simplified as:

$$q_C = h_{10} - h_7 + \eta(h_{7D} - h_{10}) \tag{14}$$

$$q_{pre3} = (h_5 - h_7) - \eta(h_{5D} - h_{10}) + \eta^2(h_{7D} - h_{10}) \tag{15}$$

$$q_{pre2} = (h_3 - h_5) - \eta(h_{3D} - h_{10}) + \eta^2(h_{7D} + h_{5D} - 2h_{10}) - \eta^3(h_{7D} - h_{10}) \tag{16}$$

$$q_{pre1} = (h_1 - h_3) - \eta(h_{1D} - h_{10}) + \eta^2(h_{7D} + h_{5D} + h_{3D} - 3h_{10}) - \eta^3(2h_{7D} + h_{5D} - 3h_{10}) + \eta^4(h_{7D} - h_{10}) \tag{17}$$

Furthermore, assuming the efficiency is infinitely approaching 100%, then Eqs. (14)–(17) become:

$$q_C = h_{7D} - h_7 \tag{18}$$

$$q_{pre3} = (h_{7D} - h_7) - (h_{5D} - h_5) = q_C - (h_{5D} - h_5) \tag{19}$$

$$q_{pre2} = (h_{5D} - h_5) - (h_{3D} - h_3) = q_C - q_{pre3} - (h_{3D} - h_3) \tag{20}$$

$$q_{pre1} = (h_{3D} - h_3) - (h_{1D} - h_1) = q_C - q_{pre3} - q_{pre2} - (h_{1D} - h_1) \tag{21}$$

And then we get:

$$Q_C = \sum_{i=1}^{3} Q_{prei} + \dot{m}\Delta h_{T_H} \tag{22}$$

where $\Delta h_{T_H} = h_{1D} - h_1$ is the integral isothermal JT effect at the ambient temperature and has a negative value.

The value of Q_C cannot be directly calculated by Eq. (22) but needs to be obtained from Eq. (5):

$$Q_C = \dot{m}q_c = \dot{m}[h_{10} - h_7 + \eta_4(h_{7D} - h_{10})] \tag{23}$$

In Eq. (23), h_{10} is determined only by the cooling temperature and its corresponding saturated vapor pressure, while h_7 is by T_{pre3} and P_U, and h_{7D} is by T_{pre3} and P_D, which are directly related to the performance of the precooling SPTC and the JT compressor. Hence, T_{pre3} and P_U exert significant influence on both the cooling capacity and the operating conditions of the entire hybrid cryocooler. In view of that, we only focus on the last stage and establish a thermodynamic model including the last stage CHEX, the JT valve and the evaporator. The gross cooling capacity is an implicit compound function of $\dot{m}$, T_C, P_U, P_D, T_{pre3}, and η_4, as shown as follow:

$$Q_C = F(\dot{m}, T_C, P_U, P_D, T_{pre3}, \eta_4) \tag{24}$$

In the following two Sections 3.2 and 3.3, we will discuss the influences of P_U and T_{pre3} on the specific cooling capacity when $T_C = 1.0$ K and $\eta_4 = 1$, namely:

$$q_C = f(P_U, T_{pre3}) \tag{25}$$

3.2. Effect of upstream pressure

Fig. 3 shows the steady state thermodynamic cycle in the *P-h* plane which indicates the change of q_C with P_U when $T_{pre3} = 8$ K. Points ***l*** and ***v*** stand for the saturated liquid and vapor state of He-3 at 1.0 K, respectively.

The isobaric specific heat capacity of the working fluid at upstream pressure and downstream pressure are C_{PU} and C_{PD}, respectively.

For He-3, the situation $C_{PU} < C_{PD}$ occurs near the cold end of the CHEX, as shown in Fig. 4. As a result, the pinch point appears at the cold end. The working fluid enters the two-phase region after throttling and becomes the mixed fluid of saturated liquid and saturated vapor. Under the condition of no heat load, the mixed fluid exchanges heat with the incoming upstream pressure hot fluid. The temperature before throttling can be cooled and infinitely approach the cooling temperature. Therefore, it is assumed that the pinch point temperature difference at the cold end of the last stage CHEX approaches to zero. Near the warm end of the CHEX, the situation $C_{PU} > C_{PD}$ occurs, which results in that the pinch point also appears at the warm end. Thus, in theory, the occurrence of a zero temperature difference at the warm end of the CHEX is possible.

Accordingly, for the throttling process, the temperature before throttling is approximately equal to the temperature after throttling, namely:

$$T_8 \approx T_9 = T_{10} \tag{26}$$

In this sense, the process of throttling expansion is not only isenthalpic but also "isothermal". And thus we get the following three conclusions under assumption of $\eta_4 = 1.0$:

(a) For process 7′→11′ in Fig. 3, q_C is equal to both q'_L and $\Delta h'_T$ as Eq. (27) shows:

$$\begin{aligned} q_C &= h_{10'} - h_{9'} = q'_L \\ &= h_{7D} - h_{7'} = \Delta h'_T \end{aligned} \tag{27}$$

This means condition of $(h'_7 - h'_8 = h_{7D} - h'_{10})$ can be used to judge Eqs. (28) and (29) [29]. The upstream pressure P'_U is an optimal pressure for the T_{pre3}.

$$h_7 - h_8 > h_{7D} - h_{10} \tag{28}$$

$$h''_7 - h''_8 < h_{7D} - h''_{10} \tag{29}$$

(b) For process 7 → 11 in Fig. 3, the upstream pressure P_U is lower than P'_U. As this condition falls in Eq. (28), q_C is equal to Δh_T.

(c) For process 7′′→11′′ in Fig. 3, the upstream pressure P''_U is higher than P'_U. As this condition falls in Eq. (29), q_C is equal to q''_L.

To sum up, under the condition that T_{pre3} is fixed, q_C is limited by both q_L and Δh_T:

$$q_C = \begin{cases} \Delta h_T & (\Delta h_T < q_L) \\ q_L & (q_L < \Delta h_T) \end{cases} \quad \text{for } T_{pre3} = \text{constant} \tag{30}$$

or

$$q_C = \min[\Delta h_T, q_L] \quad \text{for } T_{pre3} = \text{constant} \tag{31}$$

Based on the above discussions, q_C varying with P_U is calculated under the condition that $T_C = 1.0$ K and $T_{pre3} = 8$ K, as shown is Fig. 5. As P_U increases, q_C first increases and then decreases, and a maximum value $q_{C,opt} = 8.0$ kJ/kg is obtained when $\Delta h_T = q_L$ is satisfied. The

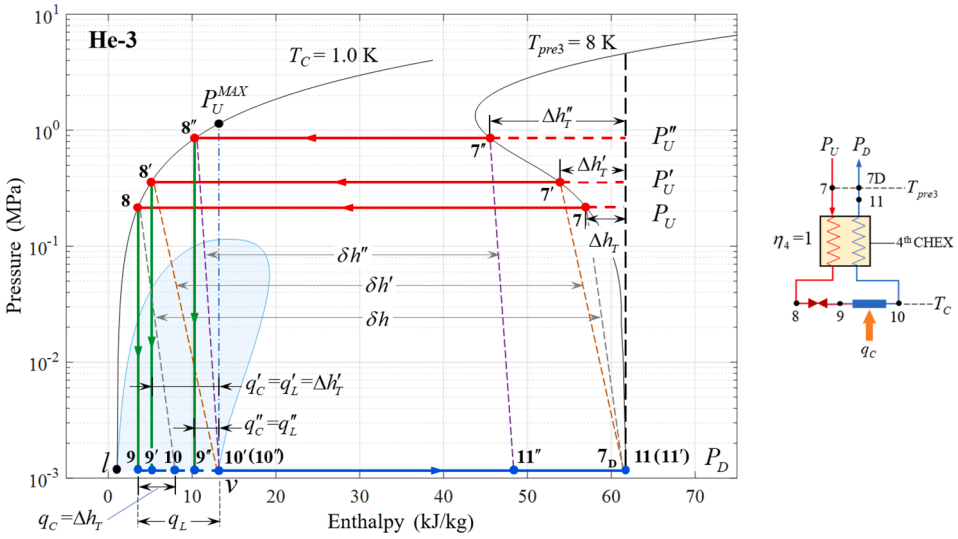

Fig. 3. Steady state thermodynamic cycle of last stage CHEX, JT valve and evaporator in *P-h* plane.

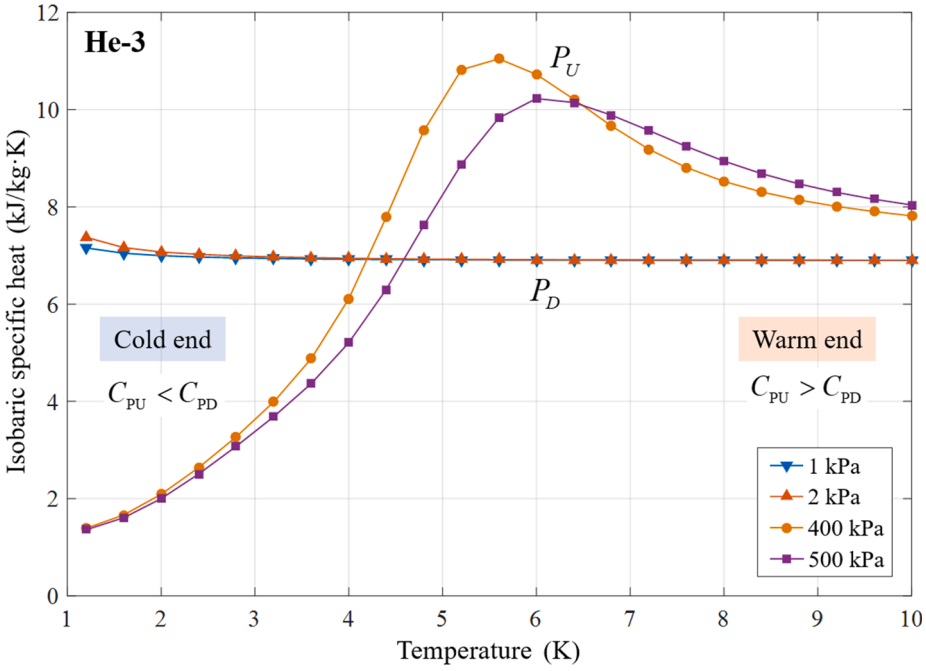

Fig. 4. Change of He-3 isobaric specific heat with temperature at different pressures.

corresponding P_U is the optimal pressure $P_{U,opt}$ = 0.36 MPa. In fact, in the low-temperature region below 30 K, the isothermal curves of He-3 at different temperatures are similar in the *P-h* diagram. Therefore, there is always an optimal P_U corresponding to a particular T_{pre3}, which means $P_{U,opt}$ can be regarded as an unary function of T_{pre3}. In addition, there is an upper limit value for the upstream pressure P_U^{MAX}. The required cooling temperature would not be obtained at any precooling temperature if P_U exceeds that value, which is determined by:

$$h(T_C, P_D) = h\left(T_C, P_U^{MAX}\right) \tag{32}$$

For T_C = 1.0 K and P_D = 1.16 kPa, the maximum upstream pressure is 1.13 MPa.

3.3. Effect of last stage precooling temperature

Fig. 6 shows the thermodynamic cycles with the change of T_{pre3} at a fixed P_U of 0.36 MPa, which indicates that T_{pre3} is another significant factor that influences q_C. The variations of q_C with T_{pre3} in terms of a series of different P_U are shown in Fig. 7.

For a constant P_U, when the condition of $\Delta h_T = q_L$ is satisfied, q_C reaches a maximum value, and the precooling temperature at the point $T_{pre3,opt}$ is the optimal value under the corresponding P_U. When the precooling temperature is below $T_{pre3,opt}$, the inequality $q_L < \Delta h_T$ holds, and thus q_C is limited by the liquefaction yield and identically equal to q_L. When the precooling temperature is above $T_{pre3,opt}$, the inequality $q_L > \Delta h_T$ holds, and thus q_C is limited by Δh_T and gradually decreases with the increasing precooling temperature until it reaches zero. Therefore, q_C can also be expressed as:

$$q_C = \begin{cases} q_L & \left(T_{pre3} < T_{pre3,opt}\right) \\ \Delta h_T & \left(T_{pre3} > T_{pre3,opt}\right) \end{cases} \quad \text{for } PU = \text{constant} \tag{33}$$

The upper limit of T_{pre3} depends on the maximum inversion

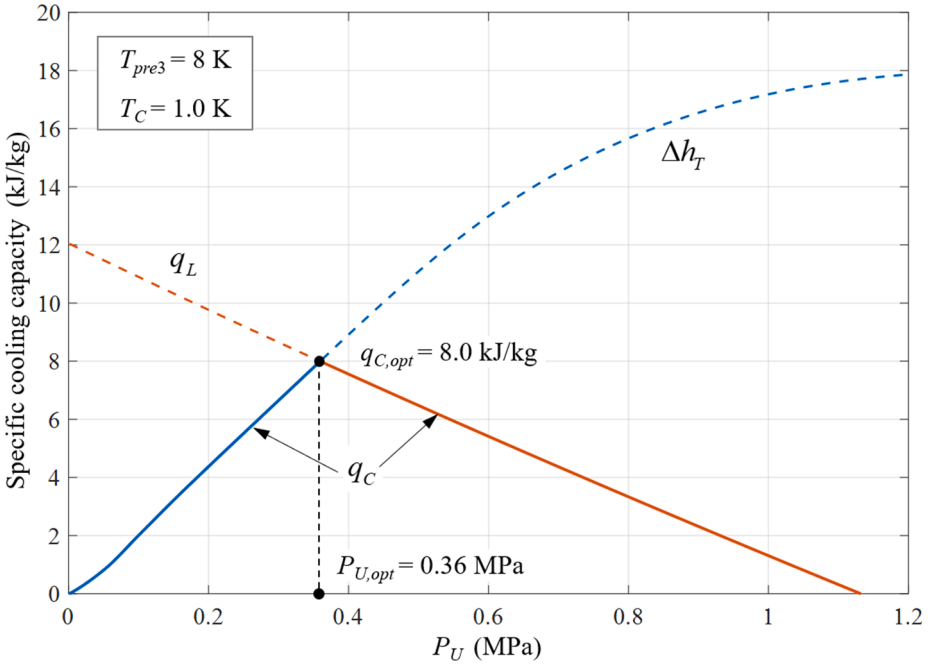

Fig. 5. Change of q_C with P_U when T_C = 1.0 K and T_{pre3} = 8 K.

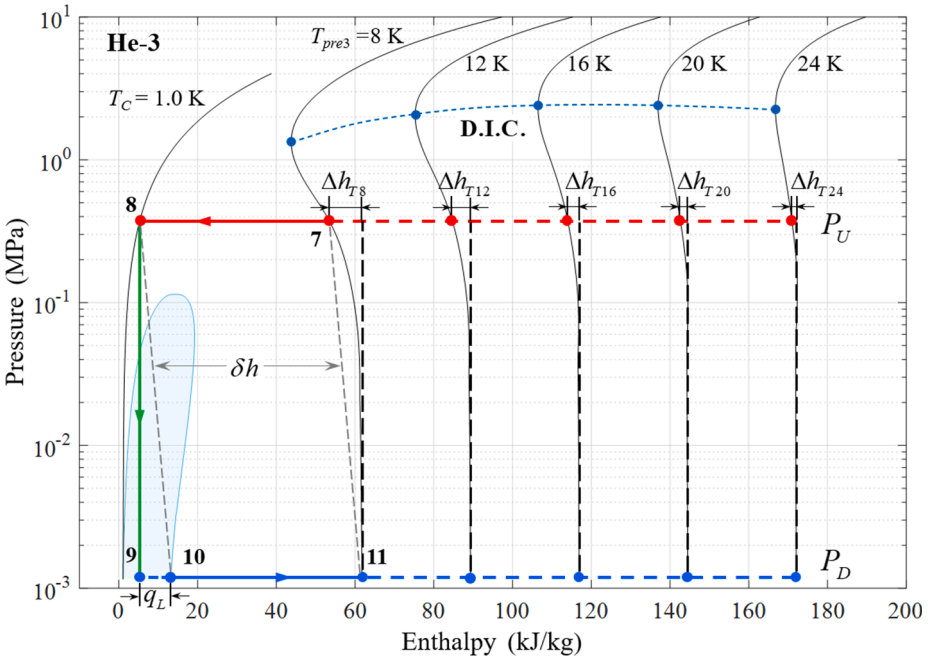

Fig. 6. Thermodynamic cycles with change of T_{pre3} when P_U = 0.36 MPa.

temperature T^{MAX} on the differential inversion curve (D.I.C.) of He-3, which means that the throttling will not produce a cooling effect if the precooling temperature exceeds that value. For He-3, the T^{MAX} is about 34 K. However, it can be observed from Fig. 6 that the cooling effect becomes considerably weak when the precooling temperature is greater than 24 K. Generally speaking, the required T_{pre3} in most practical applications is usually below 20 K.

$T_{pre3,opt}$ is a critical parameter for the coupled four-stage SPTC. Section 5 of this paper will discuss in more detail the gross cooling capacity in terms of $T_{pre3,opt}$.

3.4. Summary

Combining the above effects of P_U and T_{pre3} on q_C, it is concluded that $\Delta h_T = q_L$ is the necessary and sufficient condition for q_C to obtain its maximum value. The corresponding $T_{pre3,opt}$ and $P_{U,opt}$ are the optimal working conditions, that is:

$$q_{C,opt} = \Delta h_T(T_{pre3}, P_{U,opt}) = q_L(P_{U,opt}, T_{pre3}) \tag{34}$$

Eq. (34) indicates that the two parameters $T_{pre3,opt}$ and $P_{U,opt}$ are dependent on each other through the optimal q_C. In other words, the optimal q_C is an unary function of either $T_{pre3,opt}$ or $P_{U,opt}$. In order to investigate the characteristics of $q_{C,opt}$, T_{pre3} is selected as the

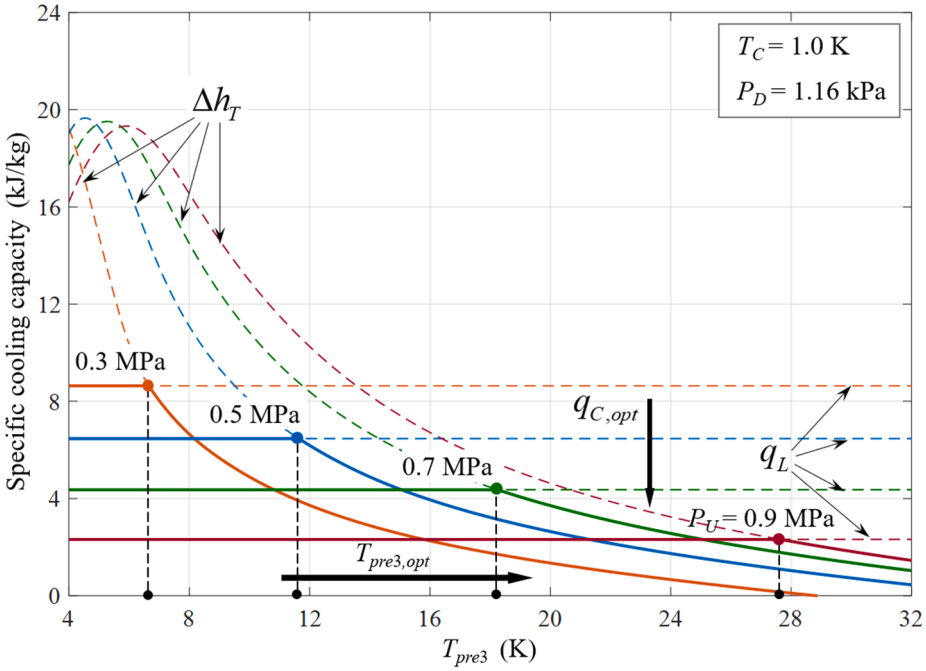

Fig. 7. Variations of q_C with T_{pre3} in terms of a series of different P_U.

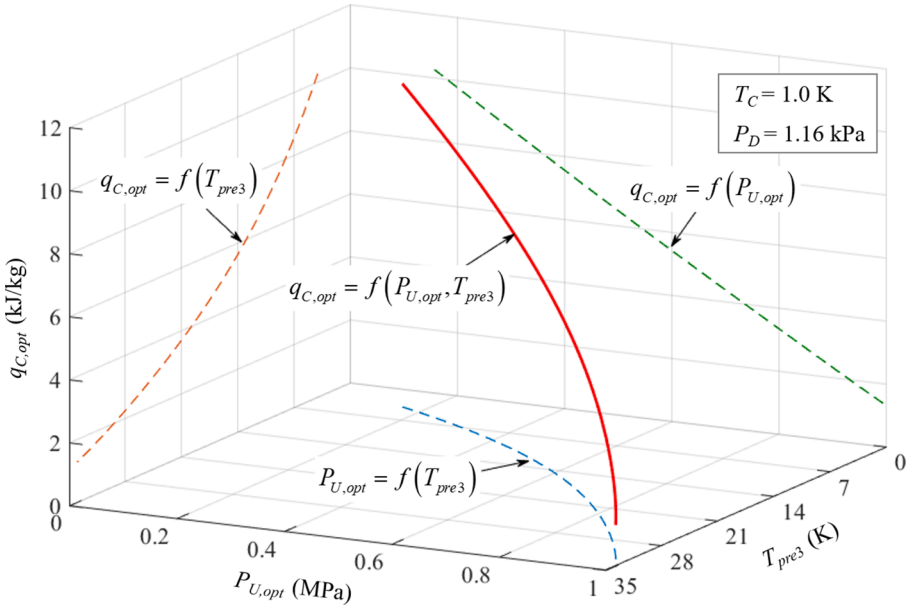

Fig. 8. Relationships between $q_{C,opt}$, $P_{U,opt}$ and T_{pre3}.

continuously changing independent variable. The relationships between $q_{C,opt}$, $P_{U,opt}$ and T_{pre3} are shown in the Fig. 8.

As T_{pre3} decreases, the corresponding $P_{U,opt}$ monotonically decreases while $q_{C,opt}$ monotonically increases. The fitting function relationship between the three is:

$$q_{C,opt} = f(P_{U,opt}, T_{pre3}) = 11.9 - 11.5P_{U,opt} + 0.027T_{pre3} \quad (35)$$

where the relationship between $P_{U,opt}$ and T_{pre3} can be expressed by a fourth power fitting function:

$$P_{U,opt} = f(T_{pre3}) = a_0 + a_1 T_{pre3}^1 + a_2 T_{pre3}^2 + a_3 T_{pre3}^3 + a_4 T_{pre3}^4 \quad (36)$$

where the coefficient values are shown in Table 1.

In practice, T_{pre3} of the SPTC is generally kept at a constant value in the steady-state operating mode. And thus both $P_{U,opt}$ and the corresponding $q_{C,opt}$ can be worked out.

Table 1
Coefficient values of Eq.(36).

a_0	a_1	a_2	a_3	a_4
−0.102	0.074	-2.37×10^{-3}	4.88×10^{-5}	-4.30×10^{-7}

4. Mass flow rate model

Based on the enthalpy flow model, the variations of q_C with parameters P_U and T_{pre3} have been discussed in the previous section. To

obtain the gross cooling capacity Q_C, another significant element, namely the mass flow rate $\dot{m}$, has to be investigated as well. Q_C can be written as follow:

$$Q_C = q_C \dot{m} \tag{37}$$

In most previous studies, $\dot{m}$ is often regarded as a given value. However, it actually is a complex function of the upstream stagnation inlet conditions, T_0 and P_0, and the throttle orifice diameter d. Therefore, Q_C should be expressed as:

$$Q_C = q_C\left(T_{pre3}, T_C, P_U\right)\dot{m}(T_0, P_0, d) \tag{38}$$

The following discussions are still based on the assumption of $\eta_4 = 1.0$.

4.1. Choked flow conditions

Fig. 9 shows the throttling process of the working fluid from point 8 to point 9 (see Fig. 1) with several thermodynamic parameters at the inlet and outlet boundaries. He-3 entering a JT valve is compressible and expands significantly as it exits into the low pressure zone inside the evaporator. Since the velocity of the fluid before throttling is quite low, the stagnation state is equivalent to the state at the flow inlet boundary, that is:

$$P_0 = P_U \tag{39}$$

$$T_0 = T_8 \approx T_C \tag{40}$$

Maytal BZ has studied the throttling process of a series of refrigerants [30]. The compressible flow expands isentropically from the stagnation state (T_0, P_0) through a series of intermediate states (T, P), with lower pressures and temperatures and finally to a state with the local speed of sound, a. While conserving energy, the velocity increases and at a certain state, it equals the local speed of sound where the Mach Number becomes unity. This state, often referred to as the "throat" (or "critical") conditions, chokes the flow and determines the mass flow rate. In practice, the inlet to outlet pressure ratio is significantly larger than the critical ratio for choked flow.

4.2. Real gas mass flux

The mass flux for an ideal gas in choked flow conditions is given by [31]:

$$G^{ID}(T_0, P_0) \equiv \frac{\dot{m}^{ID}}{A} = \kappa^{1/2}\left(\frac{2}{1+\kappa}\right)^{\frac{\kappa+1}{2(\kappa-1)}}\sqrt{\frac{MP_0^2}{RT_0}} \tag{41}$$

where A is the minimum cross section area of the passageway [31] and given by:

$$A = \frac{1}{4}\pi d^2 \tag{42}$$

M is the molecular mass of He-3, R the universal gas constant and κ the ideal gas ratio of isobaric to isochoric heat. However, due to the obvious non-ideal characteristics of He-3 under the very low temperatures, the real gas mass flux G has a deviation from the ideal one [31]:

$$G = G^{ID}\cdot\Gamma(P_0, T_0) \tag{43}$$

where Γ is the deviation factor related to the stagnation state, which means its deviation from unity is the fraction by which the real gas mass flux deviates from the magnitude of the ideal gas mass flux.

According to Section 4.1, the four variables of the choking state, (P, T, ρ, V), satisfy the following four governing equations, which are given in Ref. [30]:

$$h(P,T) + \frac{1}{2}V^2 = h_0 = h(P_0, T_0) = \text{const} \tag{44}$$

$$s(P,T) = s(P_0, T_0) \tag{45}$$

$$V = \left(\frac{\partial P}{\partial T}\right)_s = a(P,T) \tag{46}$$

$$F(P,T,\rho) = 0 \tag{47}$$

Eq.(47) is the real gas equation of state. The solution for the throat conditions is denoted by (P^*, T^*, ρ^*, V^*) which determine the choked mass flux,

$$G \equiv G^* = \frac{\dot{m}}{A} = V^*\cdot\rho^* \tag{48}$$

Unfortunately, it is inconvenient to solve G through this procedure for different stagnation parameters. Therefore, we first study the variation trend of the deviation factor with the stagnation parameters. Then the real gas mass flux can be directly calculated with Eq.(43). The calculation method of Γ is given as follows:

(1) For a specific T_0 and an arbitrary P_0, find a series of (P, T) satisfying Eq. (45), where $P < P_0$;
(2) At the same time, these (P, T) should also satisfy Eq. (44), thus different V can be obtained accordingly;
(3) Determine the unique V corresponding to P_0 by taking Eq. (46) as the constraint condition, thereby also determining the unique set (P^*, T^*), and then substitute it into Eq. (47) to obtain G;
(4) Substitute (P_0, T_0) into Eq. (41) to calculate G^{ID}, and then divide by G to get Γ corresponding to P_0;
(5) Repeat the above process to get a series of Γ corresponding to different P_0.

Fig. 10 shows the deviation factor for He-3 over a wide range of the

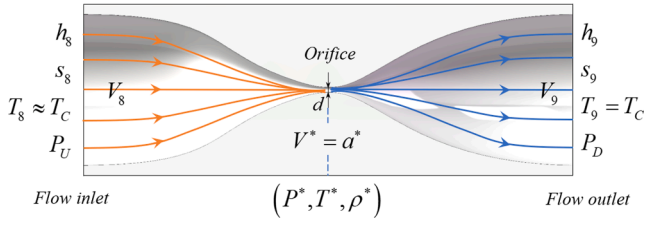

Fig. 9. Throttling process of working fluid from point 8 to point 9 (see Fig. 1) with several thermodynamic parameters at inlet and outlet boundaries.

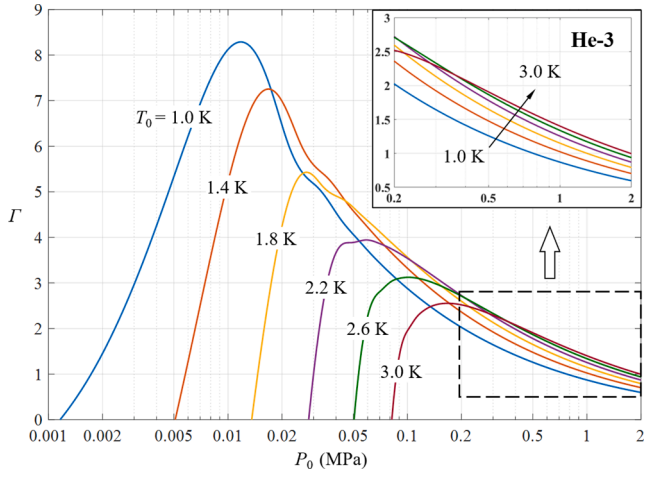

Fig. 10. Deviation factor as a function of inlet stagnation pressure and temperature with a logarithmic abscissa.

inlet stagnation pressures and temperatures. Given a constant T_0, as P_0 increases, Γ first increases sharply and then decreases slowly. In the low P_0 region of less than 0.3 MPa, the higher T_0 is, the smaller the magnitude of Γ. When P_0 is higher than 0.3 MPa, Γ related to different stagnation temperatures are relatively close. For example, given a T_0 of 1.0 K, when P_0 is 0.01 MPa, the deviation factor reaches more than 8. However, the upstream pressure of the JT cycle is generally between 0.2 MPa and 2.0 MPa. Within this range, Γ corresponding to the stagnation temperature of 1.0 K is 0.60 to 2.52, and corresponding to 3.0 K is 0.99 to 1.90. Generally, in the high P_0 region, Γ increases as T_0 rises. Substituting Γ into Eq. (43), G can be directly calculated under different T_0 and P_0 (that is, T_C and P_U).

Fitting the curves of G with P_U as the independent variable at some specific cooling temperatures from 1.0 K to 3.0 K, as shown in Fig. 11, it is found that all the fitting curves can be expressed by the following unified equations:

$$G_i(P_U) = \alpha_i P_U^{\beta_i} + \gamma_i \tag{49}$$

where i represents the condition of different T_C, and the coefficient values for different cases are shown in Table 2. For different T_C, the mass flux shows a similar change trend with the variation of P_U. In the low pressure region, G is significantly affected by the deviation factor, so there is a distinct nonlinear change. However, in the high pressure region, since the effect of the deviation factor on G weakens, the influence of the nonlinear change with P_U wanes.

5. Gross cooling capacity

So far q_C and G have been investigated, respectively, in which a number of important factors such as T_{pre3}, P_U and T_C are involved. Still, assuming that η_4 is 100%, and then the ideal gross cooling capacity Q_C can be written as the following explicit form:

$$Q_C = q_C \dot{m} = \frac{\pi}{4} d^2 G(T_C, P_U) q_C(T_C, T_{pre3}, P_U) \tag{50}$$

For the given T_C and d, for example $T_C = 1.0$ K and $d = 20$ μm, the gross cooling capacities under different operating conditions can be directly obtained by the above equation. Fig. 12 shows the relationship between Q_C and P_U at T_{pre3} of 8 K.

For the curve of $T_C = 1.0$ K, it is observed that the variation trend of Q_C with P_U is similar to that of q_C shown in Fig. 5, which increases first and then decreases. The profile of the curve varies due to the effect of the mass flow rate. Q_C reaches a maximum at P_U of 0.36 MPa, which is the same as the one corresponding to $q_{C,opt}$. At this point, the mass flow rate is 2.34 mg/s with Γ being 1.5.

Fig. 13 shows the effect of T_{pre3} on the relationship between Q_C and P_U. For the different T_{pre3}, Q_C first increases and then decreases with the increasing P_U. Therefore, there is always an optimal P_U to maximize Q_C. According to Eq.(50), the gross cooling capacity Q_C is the product of q_C and $\dot{m}$. For $T_{pre3} \geq 8$ K, when q_C is multiplied by $\dot{m}$, the monotonically increasing nature of $\dot{m}$ (see Section 4.2) has a weaker effect on Q_C than that of q_C on Q_C, hence the variation characteristic of Q_C is the same as that of q_C. In this case, the optimal P_U corresponding to Q_C exactly equals that to q_C. Therefore, $Q_{C,opt}$ increases and $P_{U,opt}$ decreases with the decreasing T_{pre3}. When $T_{pre3} = 8$ K, $Q_{C,opt}$ is 18.7 mW and the corresponding $P_{U,opt}$ is 0.36 MPa.

However, for $T_{pre3} < 8$ K, when q_C is multiplied by $\dot{m}$, the monotonically increasing nature of $\dot{m}$ has a stronger effect on Q_C than that of q_C on Q_C, especially in the region of $P_U < 0.36$ MPa, as shown in Fig. 11. In this case, the optimal P_U corresponding to Q_C no longer equals that to q_C. For example, for $T_{pre3} = 5$ K, the $P_{U,opt}$ corresponding to Q_C is 0.36 MPa while $P_{U,opt}$ to q_C is 0.21 MPa. When $P_U < 0.21$ MPa, both q_C (equals

Table 2
Coefficient values for several cases in Eq. (49).

T_C (K)	$\alpha_i \times 10^4$	β_i	$\gamma_i \times 10^3$
1.0	1.26	0.44	−0.58
2.0	1.40	0.40	−2.15
2.6	1.59	0.36	−4.36
3.0	1.82	0.32	−6.91

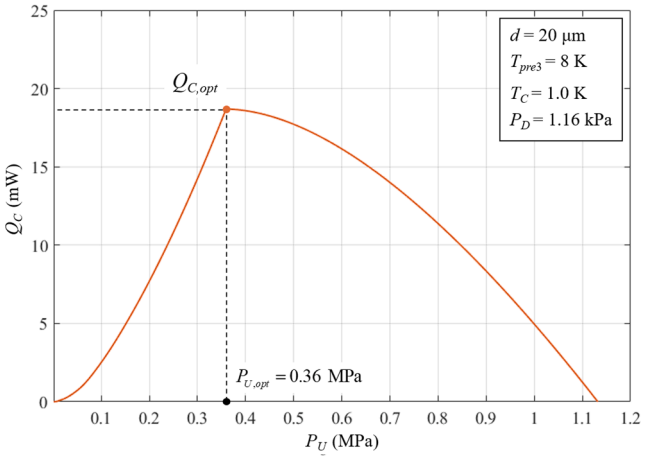

Fig. 12. Relationship between Q_C and P_U at T_{pre3} of 8 K.

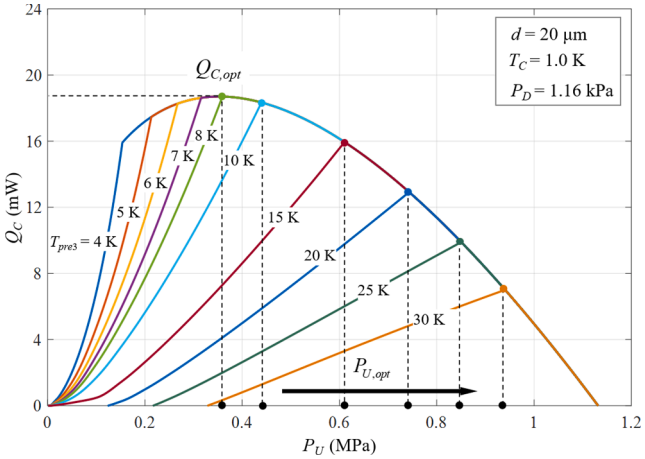

Fig. 13. Effect of T_{pre3} on the relationship between Q_C and P_U when $T_C = 1.0$ K and $d = 20$ μm.

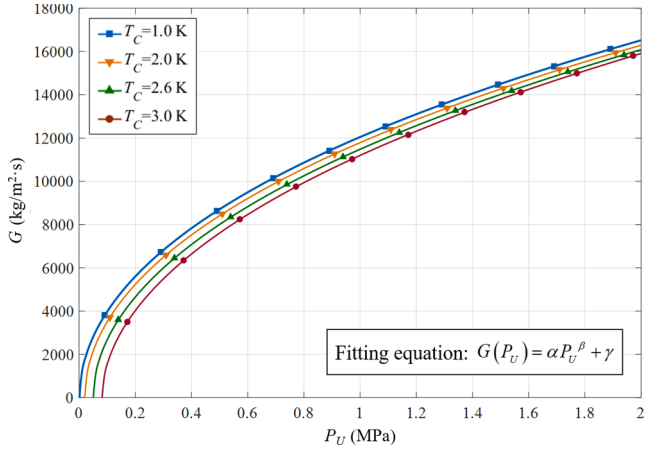

Fig. 11. Fitting curves of mass flux changing with P_U at various T_C of 1.0 K, 2.0 K, 2.6 K and 3.0 K.

to Δh_T) and $\dot{m}$ increase as P_U increases, thus Q_C increases as well. When $P_U > 0.21$ MPa, q_C (equals to q_L) begins to decrease while $\dot{m}$ still increases, which results in Q_C increasing first to the optimal value of 18.7 mW and then decreasing. The variation characteristics of Q_C for all T_{pre3} of less than 8 K are the same, and the optimal gross cooling capacity $Q_{C,opt}$ is always 18.7 mW, which means that a lower T_{pre3} does not enhance Q_C any more if P_U reaches the optimized 0.36 MPa.

In addition, for different T_{pre3}, when P_U is greater than the $P_{U,opt}$ corresponding to q_C, due to q_C is equal to q_L determined by the saturation pressure of 1.16 kPa, the calculated Q_C at any fixed P_U are all the same and consequently these curves all coincide.

In summary, the two crucial intermediate variables, the optimal T_{pre3} and the related $P_{U,opt}$ are directly linked to the cooling temperature, through which, $Q_{C,opt}$ can be established as a function of the only two parameters, namely T_C and d. In other words, once the design goal and the JT valve structure are given, the gross cooling capacity upper limit of the hybrid cryocooler is also determined accordingly.

6. Efficiency of CHEX

The above analyses are based on the assumption that all of the CHEXs have perfect efficiencies. However, it is impossible in reality, which is actually another important factor affecting the cooling performance of the hybrid cryocooler. There are always temperature differences between the warm and cold ends of each stage CHEX. At the cold end of the last stage CHEX, the temperature before throttling will be higher than the cooling temperature. On the one hand, it leads to the change of the corresponding enthalpy, thereby reducing q_C. On the other hand, it causes a change in $\dot{m}$, thereby changing Q_C. Moreover, the imperfection of other stages CHEX also results in the change of the precooling capacities. The following discussions are still under the conditions that $T_C = 1.0$ K, $T_{pre3,opt} = 8$ K and $P_{U,opt} = 0.36$ MPa.

Fig. 14 shows the influence of the fourth stage CHEX efficiency η_4 on the temperatures at the warm and cold ends of the CHEX, respectively. The temperature before throttling (T_8) and the one on the downstream side at the warm end (T_{11}) are calculated by Eq.(2) and Eq.(5). Due to the insufficient heat exchange between the hot and cold fluids, as the efficiency decreases, T_8 increases while T_{11} decreases, thereby resulting in the temperature difference between the warm and cold ends. Besides, the temperature difference at the cold end is greater than that at the warm end. Generally, the efficiency of the CHEX is required to be higher than 97%, which means the temperature differences at the cold and warm ends should not exceed 1 K and 0.2 K, respectively.

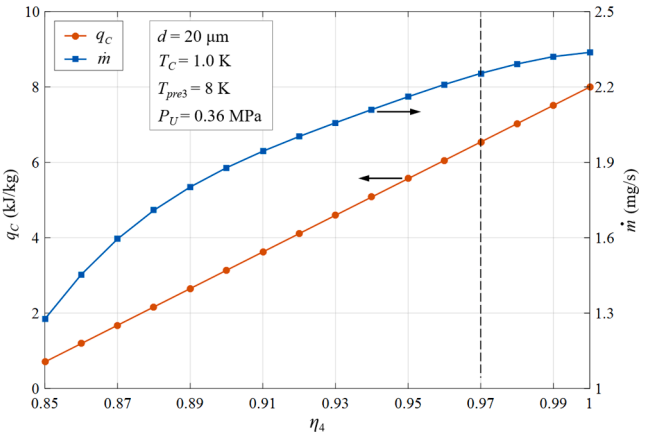

Fig. 15. Effect of CHEX efficiency on q_C and $\dot{m}$.

As shown in Fig. 15, the increase of T_8 has two results. One is that the enthalpy value increases and then q_C decreases linearly. The other is that, when T_8 (namely T_0) rises, it can be observed from Fig. 11 and calculated by Eq.(49) that G decreases at $P_U = 0.36$ MPa. Thus $\dot{m}$ declines as the efficiency decreases, and the lower the efficiency, the faster $\dot{m}$ decreases. The above two factors finally result in Q'_C decreasing

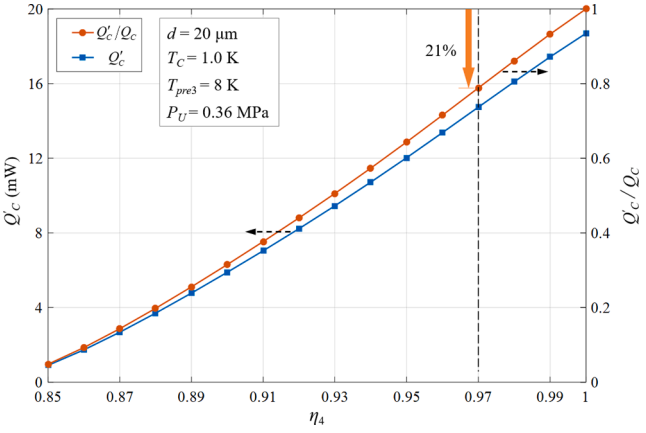

Fig. 16. Absolute and relative reductions of real Q_C with decrease of η_4.

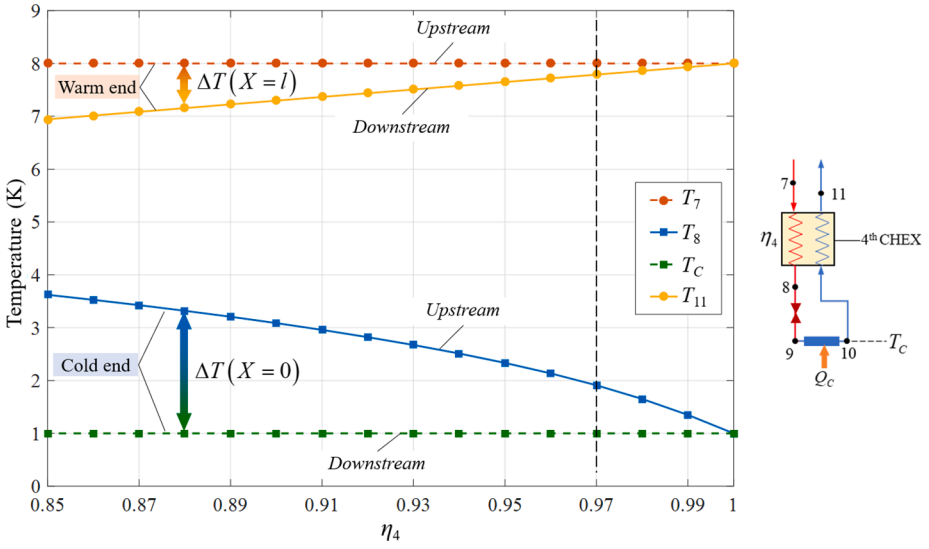

Fig. 14. Temperature variations at the cold and warm ends of the last stage CHEX with η_4 decrease.

approximately linearly with the drop of η_4, as shown in Fig. 16. For each 1% decrease of η_4, Q'_C reduces by about 7%. If η_4 reduces from 100% to 97%, Q'_C decreases by more than 20%, from 18.7 mW to 14.7 mW at 1.0 K, which proves that the efficiency of the last stage CHEX has a dramatic impact on the simulated gross cooling capacity indeed.

7. Conclusions

This paper conducts the systematic theoretical analyses of a hybrid cryocooler composed of a four-stage SPTC and a JTC, in which the former provides the necessary precooling powers to the latter which aims at reaching a temperature of 1.0 K.

The structural design of the hybrid cryocooler is described and its working mechanism focused on. Both enthalpy flow and mass flow rate models are developed and then combined to study the cooling performance. In the enthalpy flow model, the relationships among the specific cooling capacity, the last stage precooling temperature and the upstream pressure are studied, which are used to optimize the specific cooling capacity. In the mass flow rate model, the choked flow conditions are considered to obtain the real gas mass flux covering the cooling temperature from 1.0 K to 3.0 K. The ideal gross cooling capacity and its changing characteristics with both the last stage precooling temperature and the upstream pressure are elaborated. It is found that the optimal precooling temperature provided by the four-stage SPTC should be around 8.0 K with the optimal upstream pressure of 0.36 MPa to maximize the gross cooling capacity of the hybrid cryocooler at the aimed temperature.

Finally, the heat exchanger efficiency of the JTC is considered to study the hybrid cryocooler performance close to the real situation. In the simulations, Given the heat exchanger efficiencies of 97%, with He-4 in the four-stage SPTC and He-3 in the JTC, a cooling power of 14.7 mW at 1.0 K can be achieved.

The above results indicate that the suggested hybrid cryocooler would become a promising candidate for cooling the SNSPD for the potential applications in the next-generation space quantum information technology.

CRediT authorship contribution statement

Tao Zhang: Writing - original draft, Methodology, Data curation. **Haizheng Dang:** Conceptualization, Methodology, Supervision, Writing - original draft, Writing - review & editing.

Declaration of Competing Interest

The authors declare that they have no known competing financial interests or personal relationships that could have appeared to influence the work reported in this paper.

Acknowledgements

This work is supported by the National Natural Science Foundation of China (Grant No. 52076210) and Shanghai Municipal Science and Technology Major Project (Grant No. 2019SHZDZX01), and is also partly financially supported by Chinese Academy of Sciences (No. 6141A01070102) and Shanghai Municipality (Nos. 18511110100, 18511110101, 18511110102, 19511106800, 19511106801, 19511106802 and 2019-jmrh2-kj2).

References

[1] Yin J, Cao Y, Li YH, et al. Satellite-based entanglement distribution over 1200 kilometers. Science 2017;356:1140–4.
[2] Yin J, Li YH, Liao SK, et al. Entanglement-based secure quantum cryptography over 1,120 kilometres. Nature 2020;582:501–5.
[3] Zhou M, Wang W, Qu H, et al. InGaAsP/InP single photon avalanche diodes with ultra-high photon detection efficiency. Opt Quant Electron 2020;52:299. https://doi.org/10.1007/s11082-020-02422-5.
[4] Fukuda D, Fujii G, Numata T, et al. Titanium-based transition-edge photon number resolving detector with 98% detection efficiency with index-matched small-gap fiber coupling. Opt Express 2011;19:870–5.
[5] Peacock A, Verhoeve P, Rando N, et al. Single optical photon detection with a superconducting tunnel junction. Nature 1996;381:135–7.
[6] Day PK, LeDuc HG, Mazin BA, et al. A broadband superconducting detector suitable for use in large arrays. Nature 2003;425:817–21.
[7] Goltsman GN, Okunev O, Chulkova G, et al. Picosecond superconducting single-photon optical detector. Appl Phys Lett 2001;79:705–7.
[8] You L. Superconducting nanowire single-photon detectors for quantum information. Nanophotonics 2020;9:2673–92.
[9] Jia T, Wan C, Zhao L, et al. Temperature dependence of niobium superconducting nanowire single-photon detectors in He-3 cryocooler. Chin Sci Bull 2014;59:3549–53.
[10] Radebaugh R. Development of the pulse tube refrigerator as an efficient and reliable cryocooler. In: Proceedings of Institute of Refrigeration (London) 1999–2000, 2000.
[11] Kittel P. Enthalpy, entropy, and exergy flow losses in pulse tube cryocoolers. Cryocoolers 2005;13:343–52.
[12] Dang HZ. Development of high performance moving-coil linear compressors for space Stirling-type pulse tube cryocoolers. Cryogenics 2015;68:1–18.
[13] Nast T, Olson J, Champagne P, et al. Development of a 4.5 K pulse tube cryocooler for superconducting electronics. Adv Cryog Eng 2008;53:881–6.
[14] Zhi XQ, Han L, Dietrich M, et al. A three-stage Stirling pulse tube cryocooler reached 4.26 K with He-4 working fluid. Cryogenics 2013;58:93–6.
[15] Chen L, Wu X, Wang J, et al. Study on a high frequency pulse tube cryocooler capable of achieving temperatures below 4 K by helium-4. Cryogenics 2018;94:103–9.
[16] Dang HZ, Zha R, Tan J, et al. Investigations on a 3.3 K four-stage Stirling-type pulse tube cryocooler. Part A: Theoretical analyses and modeling. Cryogenics 2020;105:103014.
[17] Dang HZ, Zha R, Tan J, et al. Investigations on a 3.3 K four-stage Stirling-type pulse tube cryocooler. Part B: Experimental verifications. Cryogenics 2020;105:103015.
[18] Wang C, Lichtenwalter B, Friebel A, et al. A closed-cycle 1 K refrigeration cryostat. Cryogenics 2014;64:5–9.
[19] Liu DL, Gan ZH, Waele ATAMD, et al. Temperature and mass-flow behavior of a He-4 Joule-Thomson cryocooler. Int J Heat Mass Transf 2017;109:1094–9.
[20] Ma YX, Quan J, Wang J, et al. Development of a space 100 mW@5 K closed loop JT cooler. Cryogenics 2019;104:102983.
[21] Petach M, Casement S, Michaelian M, et al. Mechanical cooler for IXO and other space based sensors. In: AAS conference in Long Beach California; January 2009.
[22] Raab J, Tward E. Northrop Grumman Space Systems cryocooler overview. Cryogenics 2010;50:572–81.
[23] Dang HZ, Zhang T, Zha R, et al. Development of 2 K space cryocoolers for cooling the superconducting nanowire single photon detector. In: IEEE Transactions on Applied Superconductivity, Vol.29, No. 5, AUGUST 2019, doi: 10.1109/TASC.2019.2902770, 2019.
[24] Huang YH, Chen GB. A practical vapor pressure equation for helium-3 from 0.01 K to the critical point. Cryogenics 2006;46:833–9.
[25] Narasaki K, Tsunematsuet S, Ootsuka K, et al. Development of 1 K-class Mechanical Cooler for SPICA. Cryogenics 2004;22:375–81.
[26] Sato Y, Sawada K, Shinozaki K, et al. Development of 1K-class Joule-Thomson cryocooler for next-generation astronomical mission. Cryogenics 2016;74:47–54.
[27] Jahromi AE, Miller FK. Modeling, development, and experimental validation of a Joule-Thompson superfluid refrigerator using a pulse tube cryocooler. Cryogenics 2014;61:15–24.
[28] Pobell F. Matter and Methods at Low Temperatures, The third edition. Berlin: Springer; 2007.
[29] Narasaki K. Analysis of two-stage Joule-Thomson expansion. Cryogenics 2016;74:59–65.
[30] Maytal BZ. Real gas choked flow conditions at low reduced-temperatures. Cryogenics 2006;46:21–9.
[31] Maytal BZ, Pfotenhauer JM. Miniature Joule-Thomson Cryocooling: Principles and Practice. Berlin: Springer; 2013.